Observation of the dispersion relations for quantized coherent spin waves excited by a microwave antenna

Yoichi Shiota [1,*] Ryusuke Hisatomi,[1] Takahiro Moriyama [1] and Teruo Ono[1,2]

[1]*Institute for Chemical Research, Kyoto University, Uji, Kyoto 611-0011, Japan*
[2]*Center for Spintronics Research Network, Osaka University, Toyonaka, Osaka 560-8531, Japan*

The propagation of coherent spin waves in permalloy microstrips was investigated using a heterodyne-magneto-optical Kerr effect technique. The two-dimensional imaging reveals the mode interference with a high-order spin-wave mode along the microstrip width. The spin-wave dispersion relations across the microstrip width were deduced from fast Fourier transformations on the complex spin-wave amplitude of the one-dimensional scan, and multiple spin-wave modes were observed at the edges of the microstrips. These experimental results provide direct evidence for the quantization of spin-wave dispersion due to the finite width of the microstrips and enables us to evaluate the attenuation length for each quantized spin-wave mode.

I. INTRODUCTION

Spin waves and their quasiparticles, i.e., magnons, are promising for high-frequency information processing with low power consumption due to absence of charge flow and very low energy dissipation [1–3]. Using interference and nonlinear interactions, the information of spin waves allows the design of wave-based logic circuits [4]. In addition, strong couplings of magnons with other quasiparticles [5], such as microwave photons [6–10], phonons [11,12], and magnons [13–16], have attracted considerable attention for applications in quantum information processing. Furthermore, cavity optomagnonics, in which optical photons can interact with magnons through an optical cavity, have recently received great interest in realizing microwave-to-optical conversion with large-bandwidth tunability. This was first demonstrated using a ferromagnetic sphere with a submillimeter scale [17–20]. Because the coupling strength between magnons and photons is collectively enhanced by a factor of $1/\sqrt{n}$, where n is the number of spins, it can be enhanced by reducing the size of ferromagnets [18]. Very recently, improvement of the microwave-to-optical conversion efficiency has been reported, in which a ferromagnetic waveguide was used to confine both the magnon and optical modes in a small volume with large mode overlap [21]. Therefore, it is important to clarify the spin-wave modes in patterned ferromagnetic films.

The quantization effect on thermally excited spin waves was first observed using the Brillouin light scattering (BLS) technique on arrays of permalloy (Py) microstrips [22–24]. These observations have provided a basic understanding of spin-wave properties in ferromagnetic films on a microscopic scale [25]. From the viewpoint of application, it is important to investigate the coherent propagating spin waves excited by a microwave antenna. Additionally, spin-wave propagations in

materials with low Gilbert damping constant and low magnetostriction, such as Py, would be an advantage especially in a view of the rapid development of modern microwave devices [26–31]. So far, imaging of a quantized magnetostatic spin-wave mode [32], the interference of odd spin-wave modes, resulting in periodic self-focusing of spin waves [33,34], and the controlled interconversions of odd and even spin-wave modes via local magnetic fields [35] have been demonstrated. However, direct observation of the dispersion relations for quantized coherent spin waves excited by a microwave antenna has never been performed. This is because the typical setup of the micro-focused BLS technique is intrinsically incapable to detect the phase information, which is important to fully understand the dynamics of spin waves [36,37]. In this study, we investigated the antenna-excited coherent spin waves in Py microstrips with spatial resolution using a heterodyne-magneto-optical Kerr effect (MOKE) technique, and multiple spin-wave modes in the dispersion relation were directly observed at the edges of the microstrips owing to the quantization effect on the finite width.

II. EXPERIMENTAL SETUP

A film stack of Py(20 nm)/SiO$_2$(5 nm) was deposited by magnetron sputtering onto a thermally oxidized Si substrate, where the composition of Py sputtering target is Fe$_{20}$Ni$_{80}$ (in atomic %). The film was fabricated into 4 μm-wide microstrips by electron beam lithography and an Ar-ion etching technique. After depositing a 50 nm-thick SiO$_2$ layer for electrical isolation, an antenna with a ground-signal-ground coplanar waveguide to excite the spin waves was fabricated by electron beam lithography, sputtering deposition of Ti(5 nm)/Au(100 nm), and lift-off processes. An optical image and a scanning electron microscope (SEM) image of the spin-wave device used in this study is shown in Figs. 1(a) and 1(b). From SEM image, the widths of signal and ground lines for the antenna were 0.6 and 1.1 μm, respectively,
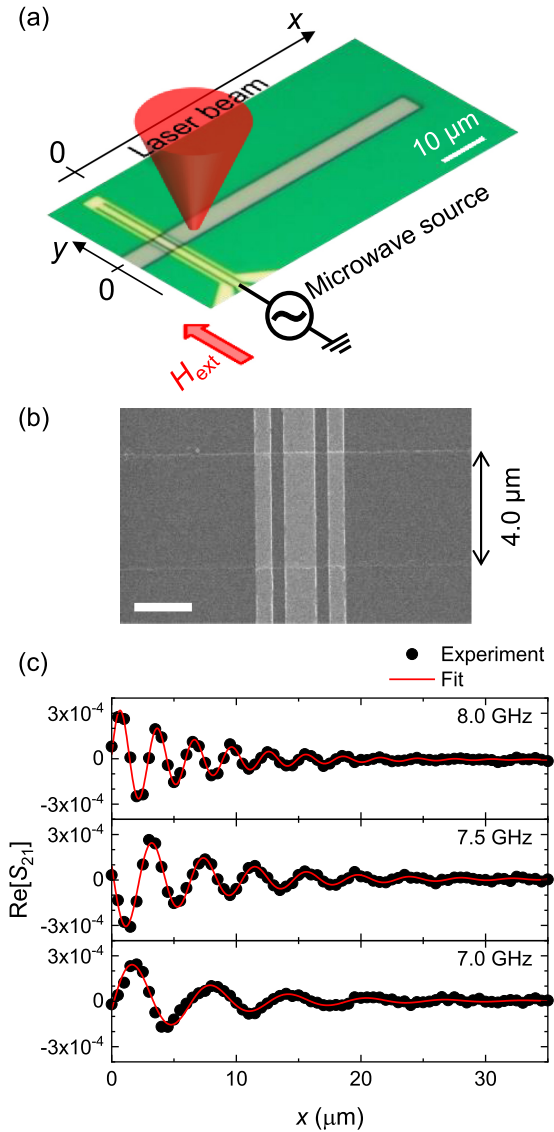
*shiota-y@scl.kyoto-u.ac.jp

FIG. 1. (a) Schematic of the spin-wave device used in the experiments. (b) Scanning electron microscope image of the Py microstrip and the antenna. The white scale bar is 2 μm. (c) Line scans of Re[S_{21}] at the excitation frequencies of 7.0, 7.5, and 8.0 GHz. Red lines represent the fittings with the exponentially decaying cosine function for evaluation of the wave number and the attenuation length at each excitation frequency.

and the edge-to-edge separation between them was 0.4 μm. The heterodyne-MOKE technique was used to investigate the spin-wave propagation in real space [38,39]. Spin waves were excited by applying microwave current to the antenna, which was connected to port 1 of a vector network analyzer. The magnetization precession dynamics were detected using a focused laser beam (wavelength, 660 nm) with linear polarization in the polar MOKE geometry. The rotation of the polarization plane in the reflected light was analyzed with a half-wave plate and a polarizing beam splitter, and detected by a high-speed photodetector. The optical heterodyne signal was sent to port 2 of the vector network analyzer, and then the intensity and phase of the propagating spin waves could be obtained from the transmitted signal S_{21} measurement. As
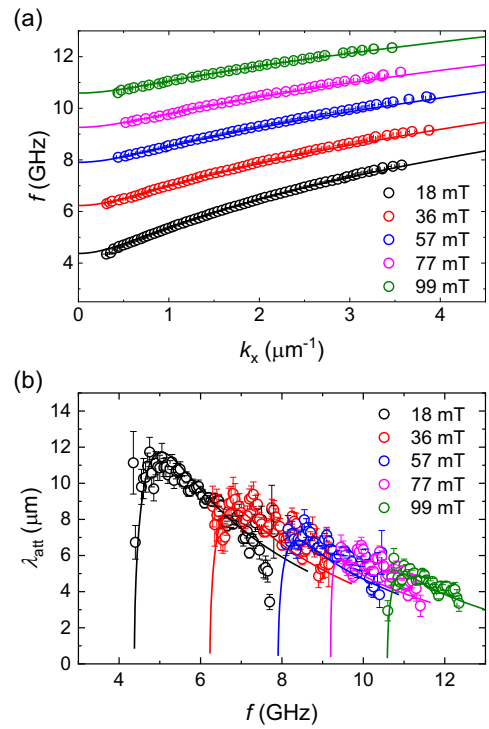

FIG. 2. (a) Spin-wave dispersion and (b) attenuation length of propagating spin waves under various magnetic fields. The solid lines in panels (a) and (b) represent the theoretical values obtained using Eqs. (1) and (2), respectively.

shown in Fig. 1(a), the spin waves propagated along the x direction, and an external magnetic field H_{ext} was applied in the y-direction. We defined the origin of the xy axis as the edge of the antenna and center of the Py microstrips. All measurements were performed at room temperature.

III. RESULT AND DISCUSSION

To investigate the propagating spin-wave properties, we investigated a one-dimensional (1D) scan at the center of the Py microstrips ($y = 0$). Figure 1(c) shows Re[S_{21}] signal under an external magnetic field of 36 mT at excitation frequencies of 7.0, 7.5, and 8.0 GHz as a function of the x position. The oscillation periods, i.e., the wavelength of the spin waves, become shorter with increasing excitation frequency, which agrees with the property of the magnetostatic surface wave mode [40]. These were fitted to an exponentially decaying cosine function, $A \cos(k_x x + \varphi)e^{-x/\lambda_{att}}$, with the fitting parameters of the amplitude A, the wave number along the x direction k_x, the excitation phase φ, and the attenuation length of the propagating spin waves λ_{att}, respectively.

The obtained k_x and λ_{att} as a function of the excitation frequency under different external magnetic field are shown in Figs. 2(a) and 2(b), respectively. As the excitation frequency increases, the wave number k_x monotonically increases, whereas the attenuation length λ_{att} rapidly increases and then slightly decreases. To quantitatively analyze the experimental data, we used the macroscopic spin-wave theory for in-plane magnetized films in the magnetostatic limit ($kt \ll 1$, where t is the thickness of a magnetic thin film).
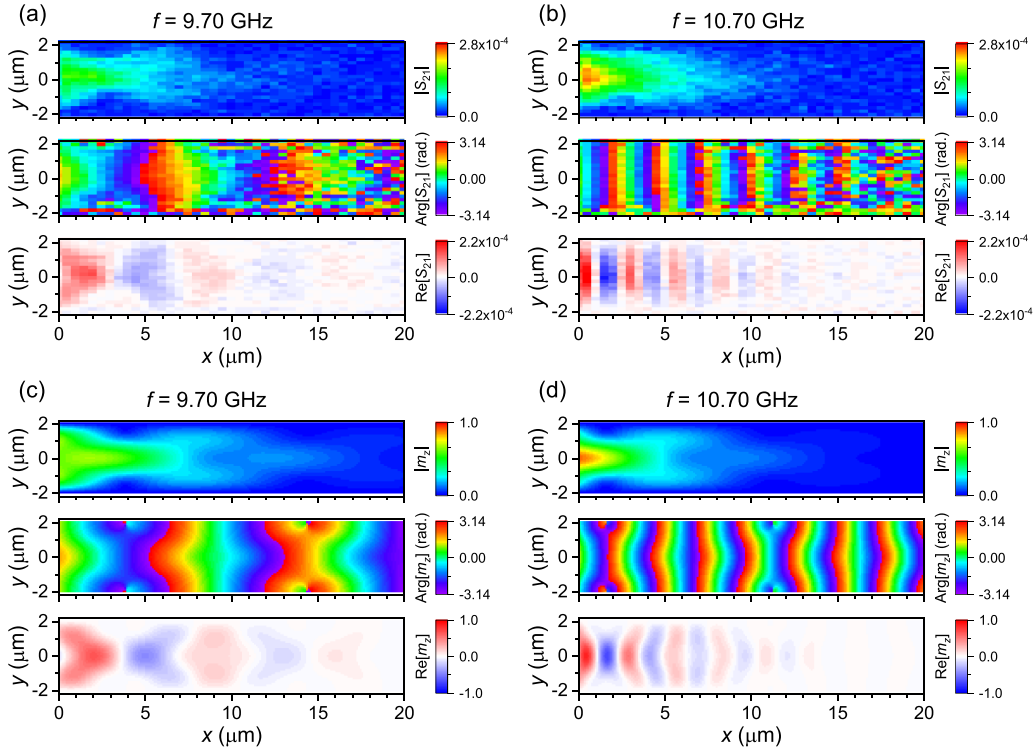
FIG. 3. (a), (b) Heterodyne-MOKE images obtained at (a) 9.70 and (b) 10.70 GHz under the magnetic field of 77 mT. (c), (d) Calculated spatial profiles of propagating spin waves for the conditions corresponding to (a) and (b), respectively, based on Eq. (4).

Because the Py microstrips have a finite size in the y direction, we assumed pinned dynamic magnetization at the edge of the strip and the cosine distribution of the magnetization amplitude in the y direction. Therefore, the wave number along the y direction is quantized as $k_{y,n} = n\pi/w$, where n is the mode index ($n = 1, 2, 3, \cdots$) and w is the width of the strip [22]. Then, the spin-wave dispersion and the attenuation length of the propagating spin waves can be described as [40,41]

$$f = \frac{\mu_0 \gamma}{2\pi} \sqrt{H_1 H_2}, \tag{1}$$

$$\lambda_{\mathrm{att}} = \frac{4\pi (df/dk_x)}{\alpha \mu_0 \gamma (H_1 + H_2)}, \tag{2}$$

with $H_1 = H_{\mathrm{ext}} + M_s P_k \sin^2\phi_{k,n}$ and $H_2 = H_{\mathrm{ext}} + M_s(1 - P_k)$. Here, μ_0 is the vacuum permeability, γ is the gyromagnetic ratio, α is the Gilbert damping constant, M_s is the saturation magnetization, and $P_k = 1 - (1 - e^{-|k_n|t})/(|k_n|t)$. To consider the standing spin waves along the y direction, the wave number k_n and the propagation angle with respect to the external magnetic field direction $\phi_{k,n}$ can be written as $k_n = \sqrt{k_x^2 + k_{y,n}^2}$ and $\phi_{k,n} = \tan^{-1}(k_x/k_{y,n})$. The solid lines in Figs. 2(a) and 2(b) represent the theoretical values obtained using Eqs. (1) and (2), respectively, for the lowest mode $n = 1$, where $\mu_0 \gamma/(2\pi) = 29.3$ GHz/T, $\mu_0 M_s = 1.23$ T, and $\alpha = 0.006$ were used. The obtained α from the attenuation length of the propagating spin waves is in good agreement with the previously reported values in Py films by ferromagnetic resonance [42].

Next, we investigated the spatial profile of propagating spin waves in Py microstrips. Figures 3(a) and 3(b) show the two-dimensional (2D) imaging of $|S_{21}|$, $\mathrm{Arg}[S_{21}]$, and $\mathrm{Re}[S_{21}]$, which correspond to the intensity, phase, and dynamic component of the propagating spin waves, respectively, under an external magnetic field of 77 mT at excitation frequencies of 9.70 and 10.70 GHz (see Movie S1 in the Supplemental Material [43] for all 2D images at excitation frequencies in the range of 9.00–11.30 GHz with 0.05 GHz steps). The images were recorded with a spatial step size of 0.5 and 0.2 μm in the x and y directions, respectively. While a plane-wave-like profile can be observed in the case of excitation at 10.70 GHz, a complicated profile can be observed in the case of excitation at 9.70 GHz. This results from mode interference with the high-order spin-wave mode along the strip width.

Because the microwave magnetic field across the antenna length can be assumed to be uniform, the lateral spin-wave mode with odd numbers n can only be excited considering the cosine distribution of the magnetization amplitude [34]. In addition, the excitation efficiency of the lateral spin-wave mode decreases with increasing n as $1/n$, which can be understood by integrating the mode profile across the strip width. Considering the above model, the z-component of the spatial profile of the lateral spin-wave mode in the microstrip can be written as

$$m_{z,n}(x, y) \propto \cos\left(\frac{n\pi}{w}y\right) \exp\left[i(k_{x,n}x - 2\pi ft + \varphi_n)\right]$$
$$\times \exp\left[-x/\lambda_{\mathrm{att},n}\right], \tag{3}$$

where $k_{x,n}$, φ_n, and $\lambda_{\mathrm{att},n}$ are the wave number along the x direction, excitation phase, and attenuation length for the nth lateral spin-wave mode at the corresponding excitation frequency, respectively. Then, the complete spatial profile of the
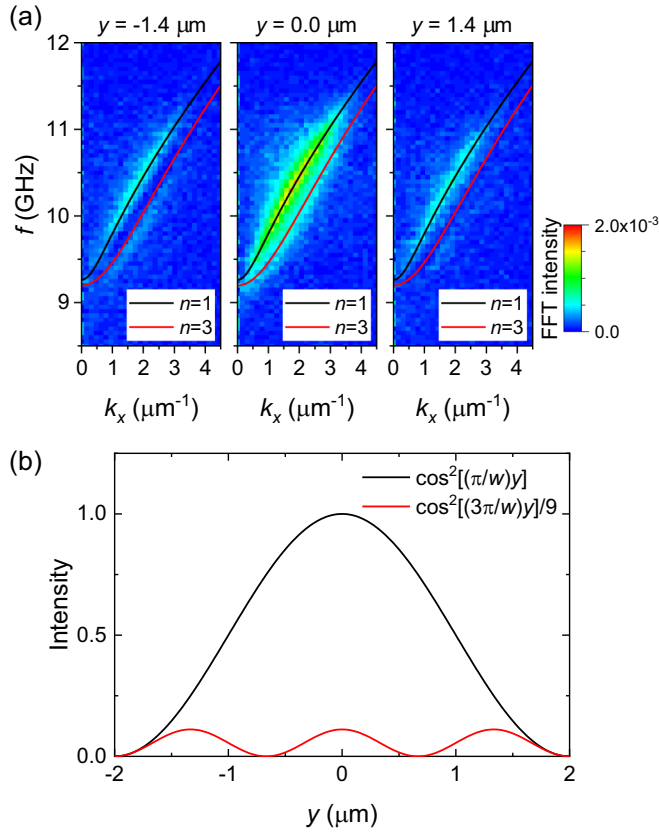
FIG. 4. (a) Contour plots of FFT extracted from the complex values of 1D scans at various y positions under the external magnetic field of 77 mT. Solid lines represent the spin-wave dispersion curves for the quantized spin-wave mode with $n = 1$ (black lines) and $n = 3$ (red lines) based on Eq. (1). (b) Calculated spatial distributions of spin-wave intensity for the modes of $n = 1$ (black line) and $n = 3$ (red line).

propagating spin waves considering the first two odd modes with $n = 1$, 3 takes the following form:

$$m_z(x, y) = m_{z,1}(x, y) + \frac{1}{3}m_{z,3}(x, y). \tag{4}$$

The calculated spatial profiles of $|m_{z,n}|$, $\mathrm{Arg}[m_{z,n}]$, and $\mathrm{Re}[m_{z,n}]$ based on Eq. (4) in the cases of 9.70 GHz and 10.70 GHz are shown in Figs. 3(c) and 3(d), respectively, where $k_{x,n}$ and $\lambda_{\mathrm{att},n}$ for the first and third spin-wave modes were determined from Eqs. (1) and (2), respectively, and $-2\pi f t + \varphi_1$ was used as the excitation phase obtained from the fitting of the 1D scan at the center of the Py microstrip φ. The interference images strongly depend on the relative phase shift between the two modes $\Delta\varphi = \varphi_3 - \varphi_1$, and $\Delta\varphi = -(3/4)\pi$ for 9.7 GHz and $\Delta\varphi = -(1/3)\pi$ for 10.7 GHz were chosen to reproduce the experimental results. Although the exact excitation theory is needed to determine $\Delta\varphi$ with respect to the excitation frequency [34], the calculated spatial profiles of propagating spin waves qualitatively agree well with the experimentally obtained ones.

To examine the spin-wave dispersion relation across the microstrip width, we performed fast Fourier transformation (FFT) on the complex spin-wave amplitude of the 1D scan along the x direction [39]. Figure 4(a) shows the results of FFT
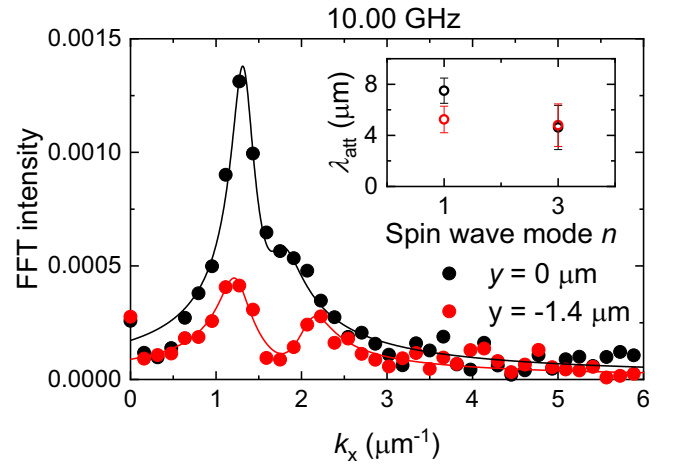

FIG. 5. FFT intensity for $y = 0\,\mu$m (black) and $-1.4\,\mu$m (red) at excitation frequency of 10.00 GHz extracted from Fig. 4(a). The solid lines are fittings of $|m_{z,n}(k_x)|$ using Eq. (5). Inset shows the spin-wave attenuation length for each mode evaluated from the fittings.

amplitude at various y positions under an external magnetic field of 77 mT. While the single peak was observed at the center of the Py microstrip ($y = 0\,\mu$m), the multiple peaks were observed at the edge of the Py microstrip ($y = \pm 1.4\,\mu$m). Neglecting the spin-wave attenuation terms in Eq. (4), we could obtain the distribution of the spin-wave intensity corresponding to the first and third modes, as shown in Fig. 4(b). Although the intensity in the first mode is larger than that in the third mode across the microstrip width, they become comparable at the edge of the Py microstrip. Therefore, quantized spin-wave dispersion with higher modes can be observed at the edges of the Py microstrip. The solid lines in Fig. 4(a) represent the spin-wave dispersion curves for the quantized spin-wave mode with $n = 1$ (black lines) and $n = 3$ (red lines) based on Eq. (1), which reproduces the experimentally obtained spin-wave dispersions.

It is interesting to note the linewidth of the obtained spin-wave dispersions, because it represents the spin-wave attenuation length for each mode. From Eqs. (3) and (4), the Fourier transforms of $m_{z,n}(x)$ yields the complex Lorentzian functions with the eigen wave number for the nth spin-wave mode $k_{x,n}$ and its attenuation length $\lambda_{\mathrm{att},n}$ as follows:

$$m_{z,n}(k_x) = \sum_{n=1,3} A_n \frac{i}{k_{x,n} - k_x + i/\lambda_{\mathrm{att},n}}. \tag{5}$$

where A_n is the amplitude of the nth spin-wave mode. Figure 5 shows the obtained spectra for $y = 0\,\mu$m and $-1.4\,\mu$m at excitation frequency of 10.00 GHz extracted from Fig. 4(a). Experimental data were well fitted by $|m_{z,n}(k_x)|$ using Eq. (5), and the spin-wave attenuation length for each spin-wave mode were evaluated, as shown in the inset of Fig. 5. While the attenuation length for $n = 3$ mode is slightly shorter than that for $n = 1$ mode at the center of the microstrip, they are comparable at the edge of the microstrip. In addition, there is slight difference of the peak position, which corresponds to $k_{x,n}$, between $y = 0\,\mu$m and $-1.4\,\mu$m, especially for $n = 3$ mode. This might be due to the small internal field close to the edges of the microstrip compared

to the center [44] and high-order spin-wave mode is more sensitive to the inhomogeneity.

IV. CONCLUSION

In conclusion, we investigated the propagation of coherent spin waves excited by a microwave antenna in Py microstrips using the heterodyne-MOKE technique. The spatial distribution of the intensity and the phase of propagating spin waves were successfully captured by this technique, and the experimental results showed excellent agreement with the numerical ones. In addition, our study provided direct measurement of the dispersion relations for quantized spin waves due to the finite width of the microstrips, which enables to evaluate the spin-wave attenuation length for each mode. Understanding of the spin-wave properties in microstrips is of importance for technical applications, such as the transmission of spin waves in magnonic devices.

[1] V. V Kruglyak, S. O. Demokritov, and D. Grundler, J. Phys. D. Appl. Phys. **43**, 264001 (2010).

[2] Y. Kajiwara, K. Harii, S. Takahashi, J. Ohe, K. Uchida, M. Mizuguchi, H. Umezawa, H. Kawai, K. Ando, K. Takanashi, S. Maekawa, and E. Saitoh, Nature **464**, 262 (2010).

[3] A. V. Chumak, V. I. Vasyuchka, A. A. Serga, and B. Hillebrands, Nat. Phys. **11**, 453 (2015).

[4] A. Khitun, M. Bao, and K. L. Wang, J. Phys. D. Appl. Phys. **43**, 264005 (2010).

[5] D. Lachance-quirion, Y. Tabuchi, A. Gloppe, K. Usami, and Y. Nakamura, Appl. Phys. Express **12**, 070101 (2019).

[6] H. Huebl, C. W. Zollitsch, J. Lotze, F. Hocke, M. Greifenstein, A. Marx, R. Gross, and S. T. B. Goennenwein, Phys. Rev. Lett. **111**, 127003 (2013).

[7] Y. Tabuchi, S. Ishino, T. Ishikawa, R. Yamazaki, K. Usami, and Y. Nakamura, Phys. Rev. Lett. **113**, 083603 (2014).

[8] X. Zhang, C. L. Zou, L. Jiang, and H. X. Tang, Phys. Rev. Lett. **113**, 156401 (2014).

[9] M. Goryachev, W. G. Farr, D. L. Creedon, Y. Fan, M. Kostylev, and M. E. Tobar, Phys. Rev. Appl. **2**, 054002 (2014).

[10] L. Bai, M. Harder, Y. P. Chen, X. Fan, J. Q. Xiao, and C. M. Hu, Phys. Rev. Lett. **114**, 227201 (2015).

[11] X. Zhang, C. Zou, L. Jiang, and H. X. Tang, Sci. Adv. **2**, e1501286 (2016).

[12] J. Li, S. Y. Zhu, and G. S. Agarwal, Phys. Rev. Lett. **121**, 203601 (2018).

[13] J. Chen, C. Liu, T. Liu, Y. Xiao, K. Xia, G. E. W. Bauer, M. Wu, and H. Yu, Phys. Rev. Lett. **120**, 217202 (2018).

[14] D. MacNeill, J. T. Hou, D. R. Klein, P. Zhang, P. Jarillo-Herrero, and L. Liu, Phys. Rev. Lett. **123**, 047204 (2019).

[15] L. Liensberger, A. Kamra, H. Maier-flaig, S. Geprägs, A. Erb, S. T. B. Goennenwein, R. Gross, W. Belzig, H. Huebl, and M. Weiler, Phys. Rev. Lett. **123**, 117204 (2019).

[16] Y. Shiota, T. Taniguchi, M. Ishibashi, T. Moriyama, and T. Ono, Phys. Rev. Lett. **125**, 017203 (2020).

[17] R. Hisatomi, A. Osada, Y. Tabuchi, T. Ishikawa, A. Noguchi, R. Yamazaki, K. Usami, and Y. Nakamura, Phys. Rev. B **93**, 174427 (2016).

[18] A. Osada, R. Hisatomi, A. Noguchi, Y. Tabuchi, R. Yamazaki, K. Usami, M. Sadgrove, R. Yalla, M. Nomura, and Y. Nakamura, Phys. Rev. Lett. **116**, 223601 (2016).

[19] X. Zhang, N. Zhu, C. L. Zou, and H. X. Tang, Phys. Rev. Lett. **117**, 123605 (2016).

[20] J. A. Haigh, A. Nunnenkamp, A. J. Ramsay, and A. J. Ferguson, Phys. Rev. Lett. **117**, 133602 (2016).

[21] N. Zhu, X. Zhang, X. Han, C.-L. Zou, C. Zhong, C.-H. Wang, L. Jiang, and H. X. Tang, Optica **7**, 1291 (2020).

[22] C. Mathieu, J. Jorzick, A. Frank, S. O. Demokritov, A. N. Slavin, B. Hillebrands, B. Bartenlian, C. Chappert, D. Decanini, F. Rousseaux, and E. Cambril, Phys. Rev. Lett. **81**, 3968 (1998).

[23] J. Jorzick, S. O. Demokritov, C. Mathieu, B. Hillebrands, B. Bartenlian, C. Chappert, F. Rousseaux, and A. N. Slavin, Phys. Rev. B **60**, 15194 (1999).

[24] Y. Roussigné, S. M. Chérif, C. Dugautier, and P. Moch, Phys. Rev. B **63**, 134429 (2001).

[25] K. Y. Guslienko, S. O. Demokritov, B. Hillebrands, and A. N. Slavin, Phys. Rev. B **66**, 132402 (2002).

[26] M. Covington, T. M. Crawford, and G. J. Parker, Phys. Rev. Lett. **89**, 237202 (2002).

[27] M. Bailleul, D. Olligs, and C. Fermon, Appl. Phys. Lett. **83**, 972 (2003).

[28] K. Sekiguchi, K. Yamada, S. M. Seo, K. J. Lee, D. Chiba, K. Kobayashi, and T. Ono, Appl. Phys. Lett. **97**, 022508 (2010).

[29] K. Yamanoi, S. Yakata, T. Kimura, and T. Manago, Jpn. J. Appl. Phys. **52**, 083001 (2013).

[30] G. Gubbiotti, L. L. Xiong, F. Montoncello, and A. O. Adeyeye, Appl. Phys. Lett. **111**, 192403 (2017).

[31] S. V. Shcherbinin, S. O. Volchkov, C. Swindells, B. Nicholson, D. Atkinson, and G. V. Kurlyandskaya, Russ. Phys. J. **63**, 1 (2020).

[32] S. Tamaru, J. A. Bain, R. J. M. Van De Veerdonk, T. M. Crawford, M. Covington, and M. H. Kryder, J. Appl. Phys. **91**, 8034 (2002).

[33] V. E. Demidov and S. O. Demokritov, Appl. Phys. Lett. **91**, 252504 (2007).

[34] V. E. Demidov, S. O. Demokritov, K. Rott, P. Krzysteczko, and G. Reiss, Phys. Rev. B **77**, 064406 (2008).

[35] Z. Zhang, M. Vogel, J. Holanda, J. Ding, M. B. Jungfleisch, Y. Li, J. E. Pearson, R. Divan, W. Zhang, A. Hoffmann, Y. Nie, and V. Novosad, Phys. Rev. B **100**, 014429 (2019).

[36] Y. Hashimoto, S. Daimon, R. Iguchi, Y. Oikawa, K. Shen, K. Sato, D. Bossini, Y. Tabuchi, T. Satoh, B. Hillebrands, G. E. W. Bauer, T. H. Johansen, A. Kirilyuk, T. Rasing, and E. Saitoh, Nat. Commun. **8**, 15859 (2017).

[37] Y. Hashimoto, T. H. Johansen, and E. Saitoh, Appl. Phys. Lett. **112**, 072410 (2018).

[38] S. Z. Baba, Y. Nakata, Y. Ito, R. Hisatomi, Y. Nakamura, and K. Usami, Phys. Rev. B **100**, 104437 (2019).

[39] Y. Shiota, S. Funada, R. Hisatomi, T. Moriyama, and T. Ono, Appl. Phys. Lett. **116**, 192411 (2020).

[40] R. W. Damon and J. R. Eshbach, J. Phys. Chem. Solids **19**, 308 (1961).

[41] B. A. Kalinikos and A. N. Slavin, J. Phys. C Solid State Phys. **19**, 7013 (1986).

[42] Y. Zhao, Q. Song, S. H. Yang, T. Su, W. Yuan, S. S. P. Parkin, J. Shi, and W. Han, Sci. Rep. **6**, 22890 (2016).

[43] See Supplemental Material at http://link.aps.org/supplemental/10.1103/PhysRevB.102.214440 for all 2D images at excitation frequencies in the range of 9.00–11.30 GHz with 0.05 GHz steps.

[44] J. Jorzick, S. O. Demokritov, B. Hillebrands, M. Bailleul, C. Fermon, K. Y. Guslienko, A. N. Slavin, D. V. Berkov, and N. L. Gorn, Phys. Rev. Lett. **88**, 047204 (2002).